Construction and Building Materials 301 (2021) 124300

Contents lists available at ScienceDirect

Construction and Building Materials

journal homepage: www.elsevier.com/locate/conbuildmat

Sisal textile reinforced concrete: Improving tensile strength and bonding through peeling and nano-silica treatment

Dimas Alan Strauss Rambo [a,*], Caroline Umbinger de Oliveira [a], Renan Pícolo Salvador [a], Romildo Dias Toledo Filho [b], Otávio da Fonseca Martins Gomes [c,d], Flávio de Andrade Silva [e], Mylene de Melo Vieira [f]

[a] Department of Civil Engineering, São Judas Tadeu University, 546 Taquari St, 03166-000 São Paulo, Brazil
[b] Department of Civil Engineering, Universidade Federal do Rio de Janeiro (UFRJ), Rio de Janeiro - RJ, Brazil
[c] Centre for Mineral Technology (CETEM), Av. Pedro Calmon, 900, Ilha da Cidade Universitária, 21941-908 Rio de Janeiro, Brazil
[d] Postgraduate Program in Geosciences, National Museum, UFRJ, Av. Quinta da Boa Vista, S/N, São Cristóvão, 20940-040 Rio de Janeiro, Brazil
[e] Department of Civil and Environmental Engineering, Pontifícia Universidade Católica do Rio de Janeiro (PUC-Rio), Rio de Janeiro – RJ, Brazil
[f] Federal University of Ceará, Campus Russas, 411 Felipe Santiago St, 62900-000 Ceará, Brazil

ARTICLE INFO

Keywords:
Sisal fabric
Nano-silica
Peeling
Yarn-matrix bonding
Microstructure
Mechanical properties
Textile reinforced concrete
Digital image correlation

ABSTRACT

This work presents an experimental investigation focused on the mechanical properties of a Textile Reinforced Concrete fabricated with bi-directional sisal fabrics treated with three different procedures. The treatments consisted of immersion in a suspension of nano-silica, mechanical peeling and mechanical peeling followed by immersion in a suspension of nano-silica. Results indicated that the treatments on the fabric influenced the cracking process of the composites and were capable to improve their post-cracking tensile strength and the yarn-matrix bonding. The combination of nano-silica and peeling treatments proved to be more effective than the treatments applied independently.

1. Introduction

Textile reinforced concretes (TRC) are cement-based composites with remarkably good tensile performance particularly attractive to produce slender elements [1]. The reinforcement of cement-based matrices with fabrics or long oriented yarns, which contain bundles of hundreds or thousands of fibers, has proven to be effective in improving the tensile strength and strain capacity of such composites [2]. These benefits are also perceived in TRC using natural fabrics [3,4,5], arousing the interest of engineers and researchers for its use in structural [6,7] and non-structural [8,9] applications.

The purpose of incorporating natural fibers such as sisal in cementitious matrices, however, is not limited to the mechanical performance of the composites. It should be noted that this class of reinforcement is biodegradable and comes from natural and renewable sources [10,11], essential material characteristics for the sustainable development of cities [12]. In addition, it has low production costs, high availability and low density. When compared to synthetic fibers, natural fibers demand about 20 to 40% of their production energy [13].

In the case of sisal fibers, the reinforcement configuration varies assuming the form of vegetable pulps [14], random short fibers [15], oriented short fibers [16], long oriented fibers [17] and fabrics [18]. Cementitious composites reinforced with continuous sisal fibers (e.g.: TRC) may present uniaxial tensile strength superior to 20 MPa [19].

According to Peled [20], the bonding mechanisms between reinforcement and matrix, which govern the mechanical behavior of the TRC, are complex and can be quite different depending on the materials employed. Aspects such as the geometry of the yarn and fabric, its composition (in terms of materials and properties), the composite production method and the presence of surface treatments can largely affect the efficiency of the multifilament yarns when embedded in a cementitious matrix.

In the case of natural fibers, specifically, hydroxyl groups present on their structures make them hydrophilic, causing the fibers to absorb large amount of water. Consequently, the hydrophilic nature of the natural reinforcement impairs a perfect adhesion across the interface

* Corresponding author.
E-mail address: dimas.rambo@saojudas.br (D. Alan Strauss Rambo).

https://doi.org/10.1016/j.conbuildmat.2021.124300
Received 2 March 2021; Received in revised form 4 June 2021; Accepted 17 July 2021
Available online 30 July 2021

with the matrix leading to failure by delamination [7]. In addition, low modulus fibers, such as sisal, are expected to present low bond with cementitious matrices [21]. Techniques such as the use of static molding pressure [22], alkali, acid and thermal treatments [23], drying/rewetting cycles [24] and carbonation cure [25], have been used in the past as ways to compensate for such deficiencies in composites reinforced with sisal fibers.

In this context, this research was proposed to evaluate the influence of three different treatments applied to sisal fabrics on the mechanical properties of a TRC. The treatments consisted of immersion in a suspension of nano-silica, mechanical peeling and mechanical peeling followed by immersion in a suspension of nano-silica. Regarding the treatment using suspension of nano-silica, the study sought to take advantage of the hydrophilic nature of sisal fibers to impregnate it with nano-particles that can react with calcium hydroxide in pore solution, forming C-S-H, favoring the adhesion between yarns and matrix.

A matrix with low calcium hydroxide (CH) content was developed and used to produce the TRC. The mechanical properties of TRC containing treated and untreated fabrics were characterized in terms of pull-out resistance, tensile strength and toughness. The mean crack spacing of the TRC was assessed using Digital Image Correlation (DIC). Finally, the yarn-matrix interfaces of the composites were investigated using Scanning Electron Microscopy with Energy Dispersive X-ray Spectroscopy (SEM-EDS). The treatments proposed were found to promote a considerable enhancement on the mechanical behavior of the TRC, influencing the cracking process and yarn-matrix bonding performance.

2. Materials

2.1. Matrix components

The cementitious materials employed to produce the matrix with low CH were a commercially available high-early strength Portland cement (from Votorantim Co., similar to a CEM I 52.5R [26]) and metakaolin (from Metacaulim do Brasil Co.), whose physical and chemical properties are summarized in Table 1. In addition, a polycarboxilate-based superplasticizer ADVA Flow 880 (from GCP Applied Technologies Co.) and natural sand with maximum particle dimension equal to 1.18 mm were used.

2.2. Sisal fabric

The sisal fabric used as reinforcement in the composites was formed by closely spaced yarns (approx. 3 yarns/cm), which in turn are composed by long twisted sisal fibers. The configuration of the fabric is presented in Fig. 1, The fabric was supplied by the Brazilian company Sisal Sul, in 1 m wide rolls.

It is important to consider that the standard sisal fabric, as received, has no coating nor surface treatment, showing equivalent properties in both directions. Therefore, such standard textile will be used as a reference (REF) for future comparisons with textiles treated with nano-silica (NS) and peeling (P). The properties of the reference sisal fabric may be found in Table 2.

Table 1
Physical and chemical properties of the cement and metakaolin.

		Cement	Metakaolin
Physical properties	Density (g/cm^3)	3.10	2.56
	Particle size dimension range (μm)	0.2–80	0.1–50
Chemical composition (%)	Al_2O_3	5.2	34.0
	CaO	63.3	0.1
	SiO_2	19.2	57.0
	Fe_2O_3	2.8	2.0
	SO_3	2.8	0.1
	Others	6.7	6.8

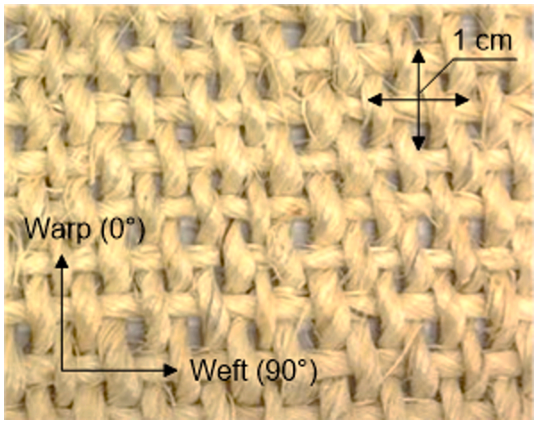

Fig. 1. Configuration of the sisal fabric used as reinforcement in the TRC.

Table 2
Properties of the reference sisal fabric.

Property	
Density of sisal (g/cm^3)	1.45
TEX (weight in grams of one km of yarn)	2676
Fabric type	Plain weave
Number of yarns per cm	~3
Coating type	None
Yarn cross section area (cm^2)	0.018
Distance between rovings (mm)	1–3
Fabric thickness (mm)	~3
Tensile strength (MPa)*	100.3
Strain capacity (%)*	7.5
Crimp index (%)	5.6
Water absorption-24 h (%)	184

*Average of four measurements.

2.3. Nano-silica

The characteristics of the suspension used as treatment in the sisal fabrics may be found in Table 3. The suspension was supplied by the Brazilian company Royal Marck, in 6 L gallons.

2.4. Treatments applied to sisal fabric

Three different treatments were used in the sisal fabrics to promote its adhesion with the matrix: treatment using immersion in a suspension of nano-silica (NS), treatment using mechanical peeling (P) followed by saturation in water and treatment using mechanical peeling followed by immersion in a suspension of nano-silica (P + NS). The reference composite was produced with the sisal fabric saturated in water (REF). Each treatment is represented in Fig. 2 and their detailed description is presented in items 2.4.2–2.4.4.

2.4.1. Reference sisal fabric (REF)

The reference sisal fabric was saturated in water until the fiber saturation point. This process prevents the fabrics from absorbing the water responsible for the mobility of the fresh matrix. The water absorption (A) was obtained from weight measurements before (w_{before}) and after immersion (w_{after}). The absorption was measured every 30 min until 3 h of immersion. After that, the intervals were extended to 1 h.

Table 3
Properties of the suspension containing nano-silica.

Solids in mass	pH	Viscosity	Density	Na_2O in mass
30%	10.5	7 mPa.s	1.2 g/cm^3	0.55%

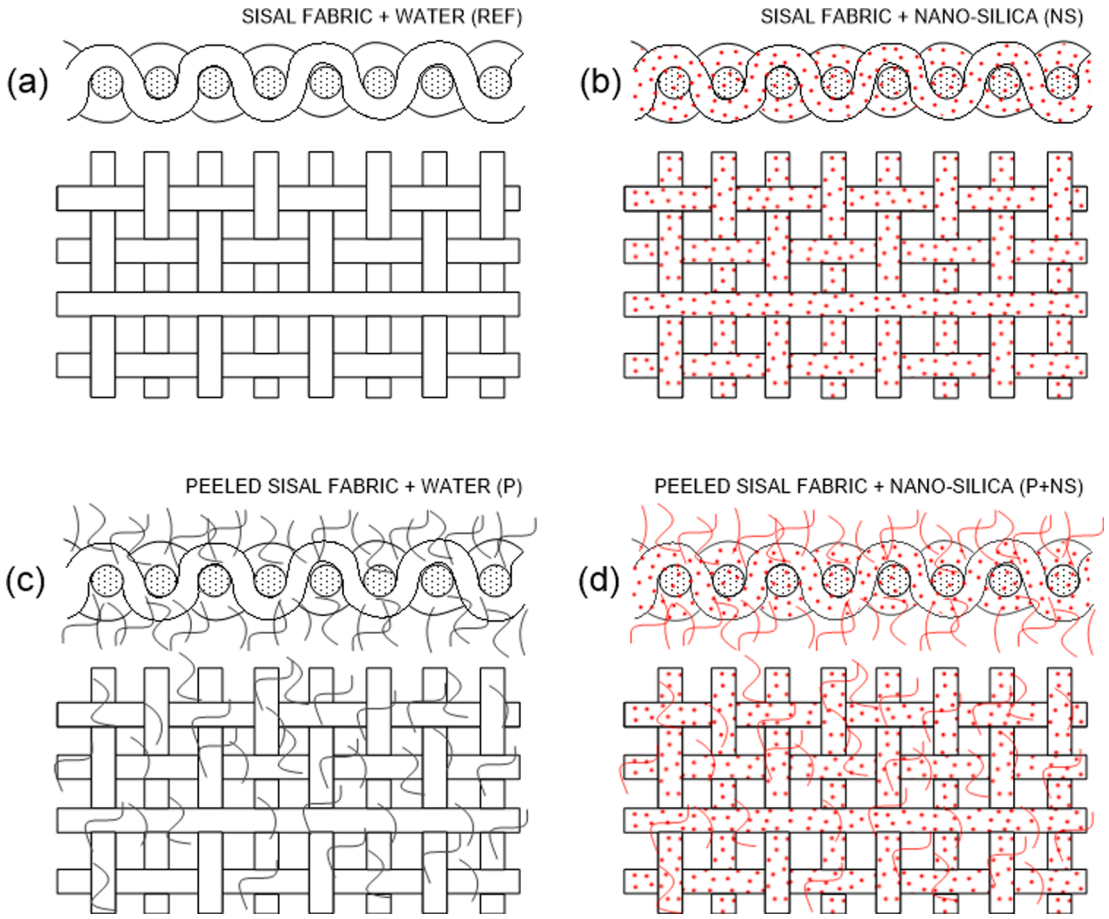

Fig. 2. Treatments applied to the sisal fabric: (a) saturation in water (REF), (b) saturation in suspension of nano-silica (NS), (c) peeling plus saturation in water (P) and (d) peeling plus saturation in a suspension of nano-silica (P + NS). The red dots and lines indicate the presence of nano-silica. (For interpretation of the references to colour in this figure legend, the reader is referred to the web version of this article.)

$$A = \frac{w_{after} - w_{before}}{w_{before}} \times 100 \quad (1)$$

In Fig. 3, it is possible to observe that the absorption curve presents three main phases, among which it is possible to identify the fiber saturation point at 8 h approximately, where the fabric showed a mass gain of 176%. After this period, the curve presented a saturation plateau, which remained practically unchanged until 24 h.

2.4.2. Treatment with Nano-silica (NS)

The untreated sisal fabric, with dimensions adjusted to the production of TRC, was immersed in plastic boxes full of suspension containing nano-silica until the fiber saturation point. This parameter was determined using the same process described in 2.4.1.

The fiber saturation point for the nano-silica treatment was reached around 8 h and 30 min, where the fabric showed a mass gain of 179% (Fig. 4). After this period, the curve presented a saturation plateau,

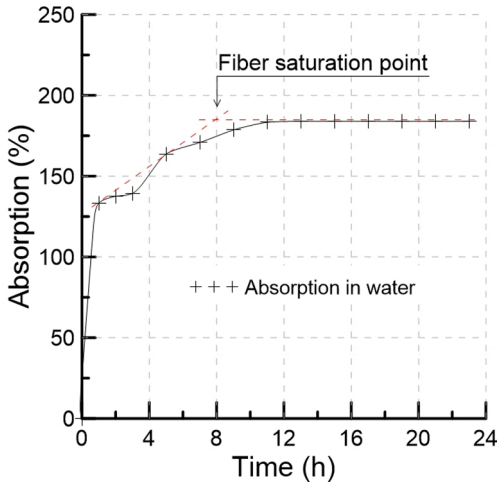

Fig. 3. Absorption of sisal fabric immersed in water.

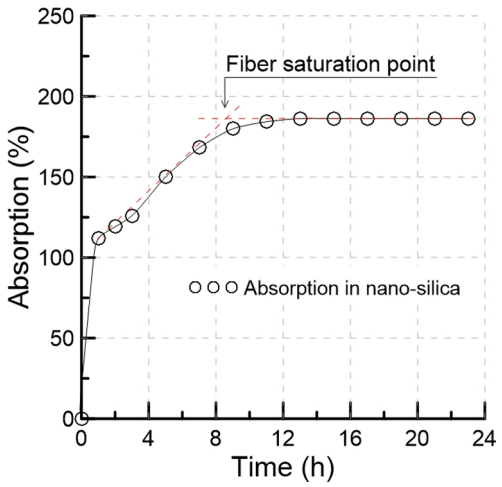

Fig. 4. Absorption of sisal fabric immersed in a suspension of nano-silica.

which remained practically unchanged until 24 h. This pattern is similar to that observed with water treatment and occurs due to the large amount of water present in the suspension (70% by mass).

2.4.3. Peeling treatment (P)

A peeling process was used to improve the bond of the fabric to the cementitious matrix, since the yarns contain a large amount of individual fibers. The peeling process contributes to detach fibers from the surface of the yarns (increasing the contact area with the matrix) and to generate a 3D feature in the reinforcement. The peeling process was done by means of a steel brush (coupled to an electric drill) being gently applied to the surface of the fabrics on both sides. Such process was maintained until the creation of a practically uniform layer of detached fibers in both surfaces. On average, the length of detached fibers (measured with a caliper) was 8 mm.

2.4.4. Treatment with Peeling + Nano-silica (TRM_P + NS)

This treatment is the combination of each treatment presented in 2.4.2 and 2.4.3. After the mechanical peeling, the fabric was saturated in nano-silica for 8 h and 30 min prior to the TRC manufacturing.

2.5. Matrix design and manufacturing

The cementitious material used to produce the matrix was composed by 60% cement and 40% metakalion (mass percentages). The unit mass proportions used were 1.0 : 1.2 : 0.35 (cementitious material : fine aggregate : water). The dosage of the superplasticizer was equal to 2.5 % by cementitious material weight. The high dosage of superplasticizer was required due to the large amount of metakaolin and to achieve the desired workability with a low water/binder ratio. The 28-day compressive strength of this matrix was 63.2 MPa, according to the standard NBR 7215 [27].

2.6. Production of TRC specimens

For each treatment applied to the sisal fabric, one rectangular panel measuring 360 mm × 200 mm × 20 mm (length × width × thickness) was produced. Each panel contained a total of three layers of the cementitious matrix and two layers of the sisal fabric. The 20 mm thickness used in the specimens is related to the thickness and number of layers of the sisal fabrics, in particular, those submitted to peeling. The fiber volume fraction on the loading direction of the specimens was calculated by the density of fibers and resulted in 3%. It is important to observe that the volumetric fraction of the natural reinforcement is not constant along the composite. This occurs in part due to the variability on the morphology properties [28] of sisal fibers which compose the yarns. In addition, the fabric manufacturing process is quite simple, and not sophisticated enough to control the volume or the number of fibers in each yarn along its length.

The experimental procedure to produce the TRC started with the matrix being disposed at the bottom surface of the mold. After that, the first layer of fabric (free of excess liquid) was positioned over the matrix. This procedure was repeated until reaching the desired number of fabric layers. The thickness of the matrix layers as well as the positioning of the fabrics were controlled by thin metal sheets (5 mm) screwed at both longitudinal sides of the mold.

Manual vibration of 1 min was applied to the molds. The TRC panels were removed from their molds 48 h after casting. The panels were then cut in four specimens measuring 360 mm × 48 mm × 20 mm (length × width × thickness), which were kept in a humid chamber (relative humidity of 90%) at 23 °C until the age of 28 days. The choice of using only three specimens per type of composite was due to problems with the alignment of the fabric close to the edges of the molds.

2.7. Production of pull-out specimens

The production of specimens destined to pull-out test started with ten twisted sisal yarns (50 cm length) being removed from each studied fabric (REF, NS, P, P + NS). After removing the yarns from the original fabrics, one of its ends was positioned along the central axis of a cylindrical mold measuring 40 mm × 40 mm (diameter × height), resulting in an embedded length equal to 40 mm. The correct positioning was conducted through two small holes created in the bottom and top covers of the molds. The yarns were then fixed at the bottom cover with a simple knot. After fixing, all yarns were lightly stretched, molds were filled with the matrix and the top cover was closed. All specimens were maintained in a humid chamber (relative humidity of 90%) at 23 °C until the age of 28 days.

2.8. Test methods

2.8.1. Thermal analysis (matrix characterization)

TGA was performed to quantify the amount of portlandite in the mortar at the age of 28 days At this age, the mortar was washed in distilled water, dried using the solvent exchange method with isopropanol and diethyl ether [29,30] and ground to a maximum particle size of 63 μm. This test was conducted from 25 to 1000 °C at a heating rate of 10 °C/min with N_2 flow of 60 mL/min using a Netzsch Libra 209 F1 thermobalance. Approximately, 50 mg of mortar were tested in 90 μL open alumina crucibles.

2.8.2. Tensile tests

Fig. 5 presents a scheme of the test set up employed for the direct tensile tests. This set up is an adaptation of the test proposed in [31]. In this case, the samples were reduced due to limitations with the test equipment. Tests were performed in a Shimadzu universal testing machine (model AGX 100 kN) coupled to a 5 kN load cell. The actuator displacement rate was 0.4 mm/min and gauge-length was equal to 130 mm. The dimensional variation of the specimens was determined by two LVDTs (from HBM Co.) positioned on both sides of the specimens. It is

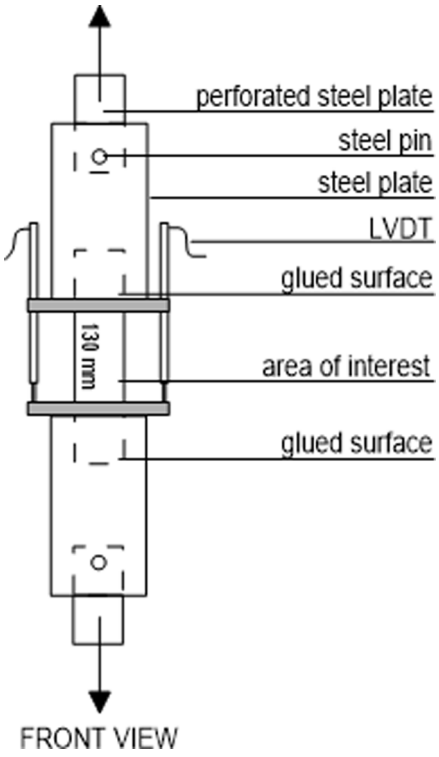

Fig. 5. Scheme of the test set up employed for the direct tensile tests.

important to remark that the tensile test used for the TRC were also employed for the matrix.

Three specimens of each composite (TRC_REF, TRC_NS, TRC_P, TRC_P + NS) measuring 360 mm × 48 mm × 20 mm (length × width × thickness) were tested. Before the tests, both ends of the TRC specimens were glued to thick steel plates (7 mm) using a high strength epoxy resin. The plates were then connected to a perforated metal plate (using a steel pin) attached to the universal testing machine through which the load was transferred to the specimens.

The evolution of the cracking process in all specimens and the average crack spacing of each group of specimens were determined by digital image correlation (DIC). The software employed uses algorithms to detect the movement of the so-called facets (default facet, 19 × 19 pixels) while the test is running. The DIC technique was applied on the tensile tests starting by capturing images of the specimen's free faces (130 mm height × 48 mm width).

Images were captured using a Nikon D90 camera with a pixel resolution of 4200 × 2690 and 10 s intervals and were imported to the software. A 2D surface component (divided in facets of 19 × 19 pixels) was created and digital image correlation was performed. The displacements (x,y) along the surface were computed and employed to obtain crack spacing values during the tests.

The speckle pattern applied to the specimens was produced by spraying white paint on the cured specimens. After that, a black paint was sprinkled on the surface with the aid of a toothbrush.

2.8.3. Pull-out tests

The pullout test used in the study was developed by the authors, and therefore does not follow any standard or recommendation. A simple scheme of the test configuration is presented in Fig. 6. Pull-out tests were performed in a Kratos universal testing machine, model KE 20000MP, coupled to a 2 kN load cell. The test was controlled by the displacement of the actuator, which was set to 4 mm/min. Ten specimens were tested for each type of sisal yarn, all at the age of 28 days. In order to favor the slipping of the yarns and, consequently, the observation of interface phenomena generated by the treatments, the embedding length adopted for the tests was 40 mm. The unembedded portion of the yarns was wound onto a steel sheave to avoid fiber damage, such as crushing and breakage, common when pneumatic grips are used.

2.9. Scanning electron microscopy with energy dispersive X-ray spectroscopy

The yarn–matrix interfaces of the composites TRC_REF and TRC_NS were investigated using a scanning electron microscope (SEM) FEI Quanta 400 with a Bruker Quantax 800 microanalysis system coupled with energy dispersive X-ray spectroscopy (EDS). SEM-EDS analysis was performed in cross-sections of these composites to evaluate the effect of the treatment using nano-silica on the interaction and load transfer among yarns, fibers and matrix.

For this analysis, cubic samples measuring 15 mm in each side were cut from the specimens used for tensile tests. Then, they were cold embedded under vacuum in epoxy resin (Struers Epofix) to form blocks with 30 mm of diameter and 20 mm height. The blocks were ground and polished in an automatic polishing machine following the traditional metallographic procedure for polished cross-section preparation [32]. The grinding was carried out using diamond impregnated metal discs with 70 μm sized diamond particles, followed by particle sizes 40, 15 and 6 μm. Water was used for cooling, and the grinding times were 2 min for the first three particle sizes and 4 min for the last one. After grinding, the blocks underwent an ultrasonic bath to remove any possible residues, to prevent scratching during polishing. The polishing procedure used cloths with diamond suspensions of 3 and 1 μm for approximately 1 h each, generating highly polished sections. Finally, the polished sections obtained were sputter coated with about 20 nm of gold to make them conductive and suitable for SEM imaging using backscattered electrons and X-ray mapping. Backscattered electrons images of polished samples are compositional images in which each pixel presents a gray level proportional to the average atomic number of its corresponding region on the specimen. Although such kind of image is useful to characterize microstructures and even sometimes identify phases, its information is not able to identify the elements present or their concentration. On the other hand, the method of X-ray mapping can reveal the elemental distribution in a polished sample typically with a resolution of about 1 μm. EDS X-ray mapping can produce simultaneously images in which the gray levels denote the concentration of different elements. Moreover, any three elemental maps can be combined by assigning each one to one of the three primary colors (red, green, and blue) to reveal the combination of those elements in different phases through a common RGB colour image [33].

3. Results and discussion

3.1. Thermal analysis (matrix characterization)

Fig. 7 presents the TG and DTG curves of the matrix analyzed. The TG curve shows a constant mass loss during the period of the test. The DTG curve identifies a shoulder from 434 to 471 °C, which corresponds to the mass loss caused by the dehydration of portlandite. This process indicates that the matrix contains 1.63% of portlandite by mass. As a reference, a mortar produced with no metakaolin and analyzed by TGA using the same procedure contains 5.34% of portlandite by mass. Therefore, it may be concluded that 70% of the portlandite was consumed due to the pozzolanic reaction of metakaolin.

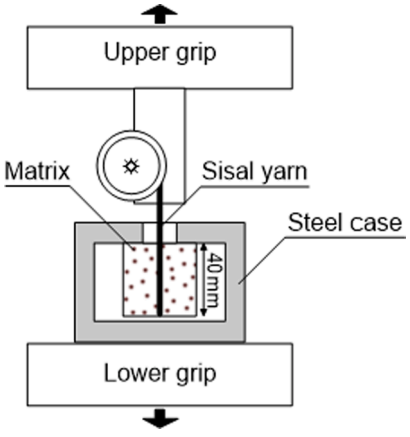

Fig. 6. Scheme of the test set up employed for the pull-out of the sisal yarns.

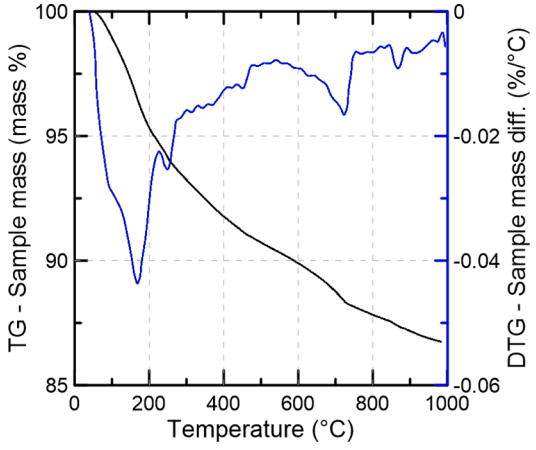

Fig. 7. TG and DTG curves of the matrix analyzed.

3.2. Sisal TRC tensile behavior

The stress–strain curves of the sisal TRC (up to 4% strain) are presented in Fig. 8. Average data regarding first crack strength (σ_{BOP}) and toughness (T) for different strain levels (0.5%, 1%, 2%, 3% and 4%) are presented in Table 4.

As expected, the treatments using nano-silica (NS), peeling (P) and the combination of both (P + NS), influence the tensile response of the composites. The average stress levels achieved at the bend-over point by the matrix showed to be higher than that observed for the TRC. This behavior reflects the inclusion of porous sisal yarns, with low modulus, in the resistant section of the samples.

TRC_REF and TRC_NS presented strain softening behavior, while TRC_P and TRC_P + NS exhibited strain hardening (with large cracks). The curves of the reference composite (TRC_REF) present an abrupt stress drop after the first crack formation. With increasing strain, debonding progresses, resulting in few wide cracks formed along the longitudinal direction of the specimen. Such pattern results from several aspects related mainly to the sisal fabric. Among them, it is possible to indicate: the dimensional instability of fibers [34] the high strain capacity presented by the sisal fabric (7.5%, Table 2); the low bond and consequent interfacial debonding occurred between the fabric and matrix under tension (common for low modulus fibers) [17] and the crimp effect related to the fabric architecture [32].

It is important to mention that, in the case of natural fiber reinforcement, especially those using plane wave fabrics, wide cracks are formed due to the crimp effect [35]. Even in the case of fabrics with greater stiffness and tensile strength (e.g.: basalt and kevlar), this phenomenon can be clearly perceived [36,37]. The crimp index calculated for the sisal fabric used indicates that the sisal yarns, when straight (with no crimp), are on average 5.6% larger than the crimped ones.

On the stress–strain curves presented by the TRC_NS (see Fig. 8 - b), it is possible to detect a lower stress drop right after the first crack in

Table 4
Average results obtained from tensile test performed on Sisal Textile Reinforced Concretes. Standard deviation values are presented in parentheses.

Composites	Tensile stress	Toughness					ANC*
	σ_{BOP}(MPa)	$T_{0.5\%}$ (J)	$T_{1\%}$ (J)	$T_{2\%}$ (J)	$T_{3\%}$ (J)	$T_{4\%}$ (J)	
Matrix	2.5 ± 0.6	0.01 ± 0.01	0.01 ± 0.01	0.01 ± 0.01	0.01 ± 0.01	0.01 ± 0.01	1
TRC_REF	1.9 ± 0.3	0.20 ± 0.04	0.6 ± 0.1	1.5 ± 0.03	2.4 ± 0.2	3.3 ± 0.4	5
TRC_NS	1.5 ± 0.2	0.30 ± 0.01	0.79 ± 0.02	1.6 ± 0.1	2.5 ± 0.1	3.3 ± 0.2	8
TRC_P	1.6 ± 0.2	0.36 ± 0.1	0.75 ± 0.4	1.6 ± 0.4	2.9 ± 0.3	5.0 ± 0.2	2
TRC_P + NS	1.8 ± 0.1	0.62 ± 0.1	1.36 ± 0.2	3.2 ± 0.7	4.9 ± 1.3	6.8 ± 1.9	9

*Average number of cracks

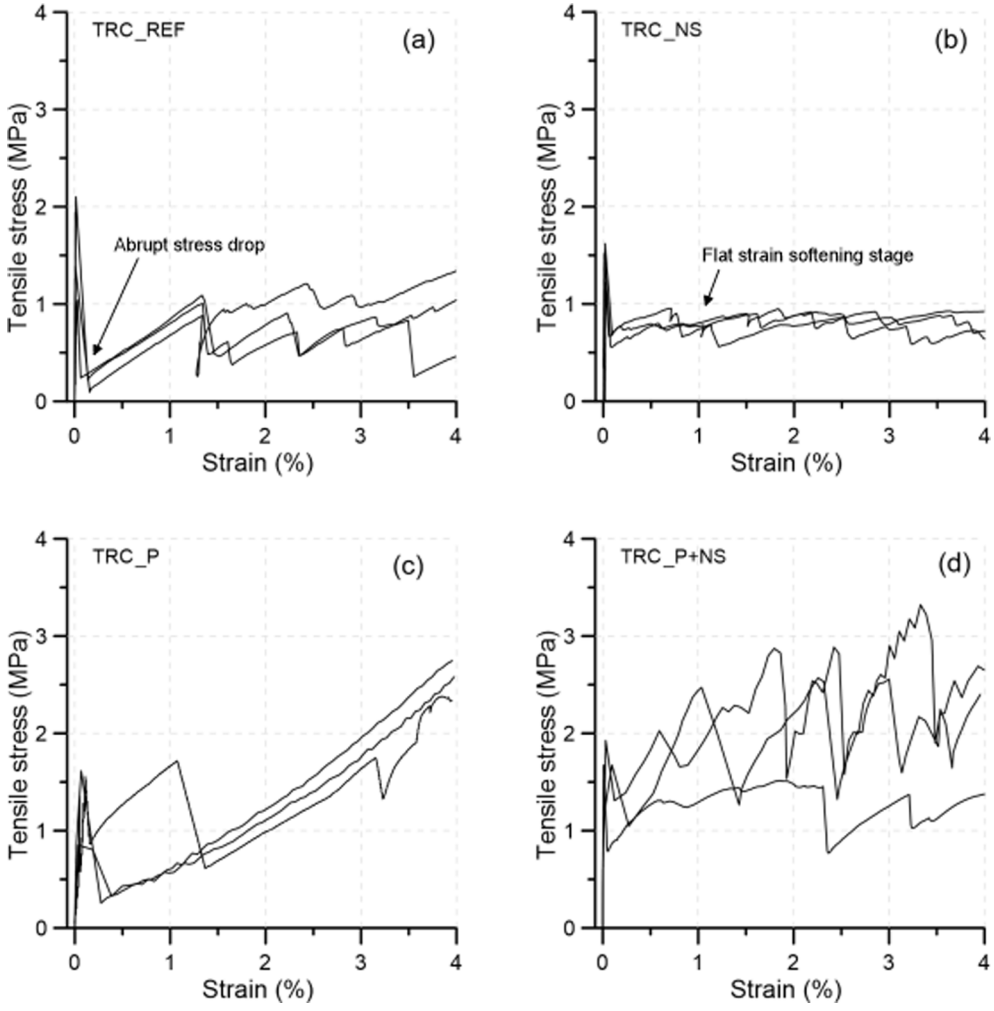

Fig. 8. Tensile stress *versus* strain curves of Sisal Textile Reinforced Concretes: (a) TRC_REF, (b) TRC_NS, (c) TRC_P and (d) TRC_P + NS.

comparison to the reference. In addition, a trend of maintenance of the post-cracking strength (flat strain softening stage) is observed. Such distinct behavior and enhanced $T_{3\%}$ are attributed to improvements in the yarn-matrix adhesion (i.e.: adhesional shear bond strength and frictional shear strength [38]), achieved by pozzolanic activity of nano-silica.

Analyzing the results obtained with TRC_P, a remarkable improvement in the composite strength and $T_{4\%}$ are obtained, when compared to the reference. The mechanical anchoring provided by peeling was able to reduce the low fiber–matrix adhesion characteristic of natural reinforcements [29]. The increase in the post-cracking strength was high enough to make the composite exhibit a strain hardening response, quite uncommon for composites reinforced with lignocellulosic fibers.

The average accumulated $T_{4\%}$ obtained by the TRC_P was 1.5 times higher than that observed for both TRC_REF and TRC_NS. The enhanced energy absorption capacity is attributed to the increase of the effective surface area of the yarns and fibers [39] in contact with the matrix. Moreover, the fibrillation and detachment of fibers from the surface of the fabrics changes the 2D nature of the reinforcement to a 3D arrangement, similar to the combined use of fabrics and short fibers. This characteristic contributes to improve mechanical anchoring of the yarns, as well as to increase the toughness of thin composites at low levels of deformation [40].

From Fig. 8 – d, it is possible to percept that the combination of nano-silica and peeling treatment significantly improved the tensile performance of TRC_P + NS. In addition to achieving a strain hardening behavior, their $T_{4\%}$ more than doubled in comparison to TRC_REF. These findings are in accordance with the aforementioned improvements achieved by both treatments, nano-silica and peeling, independently.

Representative curves of crack spacing *versus* strain and the distribution of the displacement field up to 4% strain are presented in Fig. 9. Such curves were obtained from DIC analysis for all composites. The only exception was the composite TRC_P, whose specimens did not present a sufficient number of cracks (up to 4% strain) for the calculation of the mean crack spacing.

The curves presented in Fig. 9 indicate that the treatments using nano-silica, peeling and the combination of both were capable to influence the crack pattern of the specimens. In the case of TRC_NS and TRC_P + NS, the number of macro-cracks was considerably higher than that observed for the reference, resulting in lower values of average crack spacing. From Fig. 9-b, it is possible to see that the crack evolution of these composites, TRC_NS and TRC_P + NS, behaves similarly. However, the values of crack spacing in TRC_REF were considerably higher, especially for strain levels lower than 2%. The saturated average crack spacing was approximately 20 mm for all composites tested up to 4% strain. It is important to note that the crack spacing values of the TRC_REF, at 4% strain, would have been much higher (e.g.: >30) if the cracks of the specimens had not been concentrated at their ends, a fact that occurred in all samples tested (see Fig. 9-b).

Although the specimens were not analyzed until their complete collapse, it is important to mention the differences observed in the failure modes. In the case of TRC_REF and TRC_P, the failure mode occurred close to the metal plates. After that, the pull-out of the fabric could be observed. In these cases, the anchorage length and the yarn-matrix adhesion were not sufficient to cause fabric rupture. In the case of TRC_NS and TRC_P + NS, the point of failure in the specimens proved to be random, resulting in rupture of the yarns.

It is also worth noting that in general the scale effect positively affects the mechanical response of small specimens (case of this study). This fact must be taken into account when comparing these results with other publications.

3.3. Pull-out tests

Fig. 10 depicts the peak pull-out loads of the treated and untreated sisal yarns when removed from the matrix. From the results, it is possible to note that the highest pull-out loads are observed for the yarns P + NS (average value 223 N). The average pull-out performance of this composite was enhanced in comparison to the yarns P, NS and REF by 7%,

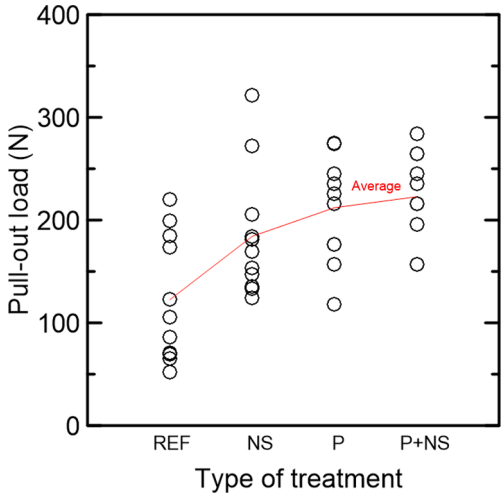

Fig. 10. Pull-out loads of treated and untreated sisal aligned sisal yarns.

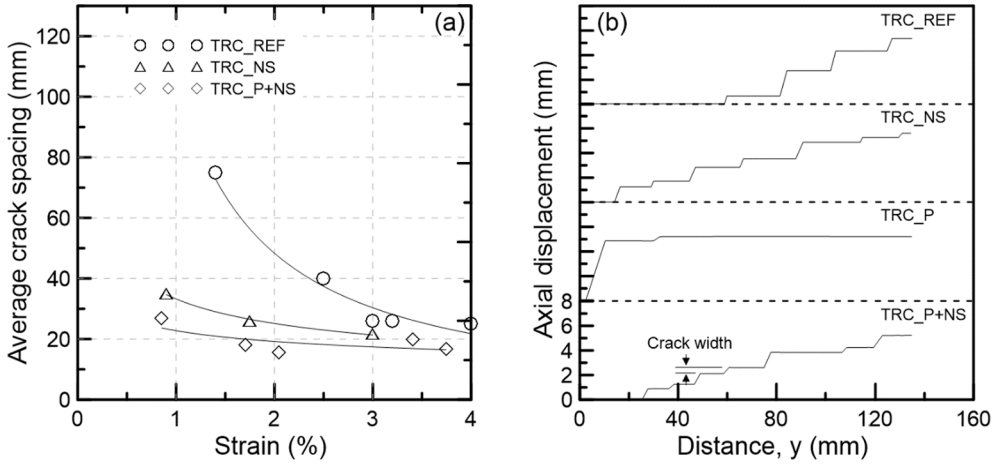

Fig. 9. (a) Crack spacing *versus* strain responses for TRC_REF, TRC_NS and TRC_P + NS; (b) Distribution of the axial displacement along the loading direction (y) for all composites.

21% and 82%, respectively. Such findings are in agreement with the tensile test results since the highest accumulated toughness values were obtained for the composite TRC_P + NS.

The average pull-out load obtained for the yarns subjected to the peeling process was 209 N. This result, similar to that obtained for P + NS, indicates that the peeling contribution is very relevant in relation to pull-out loads (more relevant than the isolated use of nano-silica saturation). These results again are in agreement with the pattern observed in the TRC toughness values.

The low pull-out performance of the REF yarns (average value 123 N) might be attributed mainly to its dimensional instability, typical in the case of vegetable fibers [29]. As well as wood or pulp fibers, sisal fibers swell when saturated. Their cross section may change dramatically, depending on the degree of fiber saturation and factors related to the matrix. This process leads to yarn debonding manly in the case of absence of hydrated products such C-S-H formed in interior of the sisal yarns. As revealed in the pull-out results, in the case of P yarns, the debonding process is compensated, becoming less evident.

3.4. SEM-EDS analysis

Fig. 11 presents the SEM images obtained with TRC_REF coupled with the X-ray mapping of calcium, silicon and carbon. The REF yarns showed to be partially hollow and depopulated of Ca and Si along the core. The low penetration of ions and compounds in the yarn core resulted in a weak yarn-matrix adhesion which was also responsible for the large stress drops presented by the TRC_REF under tension, as well as the low pull-out loads presented by REF sisal yarns (see Section 3.3).

This type of behavior is characteristic of composites reinforced with sisal fibers saturated in water. During saturation, the hydrophilic nature of the sisal reinforcement causes the yarns to become reservoirs of water which is subsequently released for both hydration and environment (i.e.: moisture equilibrium). In this process, the sisal fiber shrinks, leading to a partial debonding along the matrix interface and a consequent weakening of the interfacial transition zone [29].

In contrast to these findings, in the polished section of the TRC_NS (see Fig. 12), the yarns showed a high amount of Si and Ca along the yarn core. Such abundance of these elements suggests pozzolanic reaction of the nano-silica with calcium hydroxide (CH). Although non-uniform, the filled area between individual fibers indicates a relevant yarn-matrix interaction, which is in accordance with the improvements observed in the pull-out behavior and tension tests. In addition, it is believed that the use of nano-silica may prevent the mineralization process [41] and consequent embrittlement of the sisal reinforcement.

It is also important to note that, in general, Si and Ca fill the spaces between the fibers and not their inner core. Such process, visible in Fig. 13, can prevent the embrittlement of the fibers, enhancing mechanical properties and toughness of the composites [42].

In the case of the TRC_P + NS, not evaluated by SEM-EDS, it is believed that the growth of cement hydration products favored by the presence of nano-silica was extended to the detached fibers. As a result, mechanical anchoring and interlocking were benefited, resulting in important contributions to the pull-out response and tensile performance.

Although the nano-silica treatment enhanced the mechanical behavior presented by TRC_NS and TRC_P + NS, it is believed that the inclusion of yarns "fully saturated" has also decreased the potential strength gain of the composites. This is attributed to the excess of water present in the yarns, which yields higher water/binder ratios at the yarn-matrix interfaces [43]. This fact, added to fiber shrinkage [29], reduces the efficiency of the treatment on the mechanical performance of the composite. In addition, the dried nano-silica tends to agglomerate, forming fragile segmented blocks around the sisal fibers. This fact is clearly visible in Fig. 13. As reported by Peled et al. [38], the formation of these nano-silica clusters can reduce the potential pozzolanic effect of nano-silica resulting in decreases of the composite mechanical behavior.

4. Conclusions

The treatment using immersion of sisal fabric in suspension of nano-silica provided a constant post-crack stress (flat strain softening stage) in the composites subjected to direct tension. In addition, the number of cracks of this composite was considerably higher than the reference one. This behavior is attributed to the pozzolanic reaction of nano-silica evidenced by the improvements on the yarns' pull-out resistance and SEM-EDS analysis (massive presence of Si and Ca in the yarn core and fiber–matrix interface).

The mechanical anchoring provided by peeling was capable to

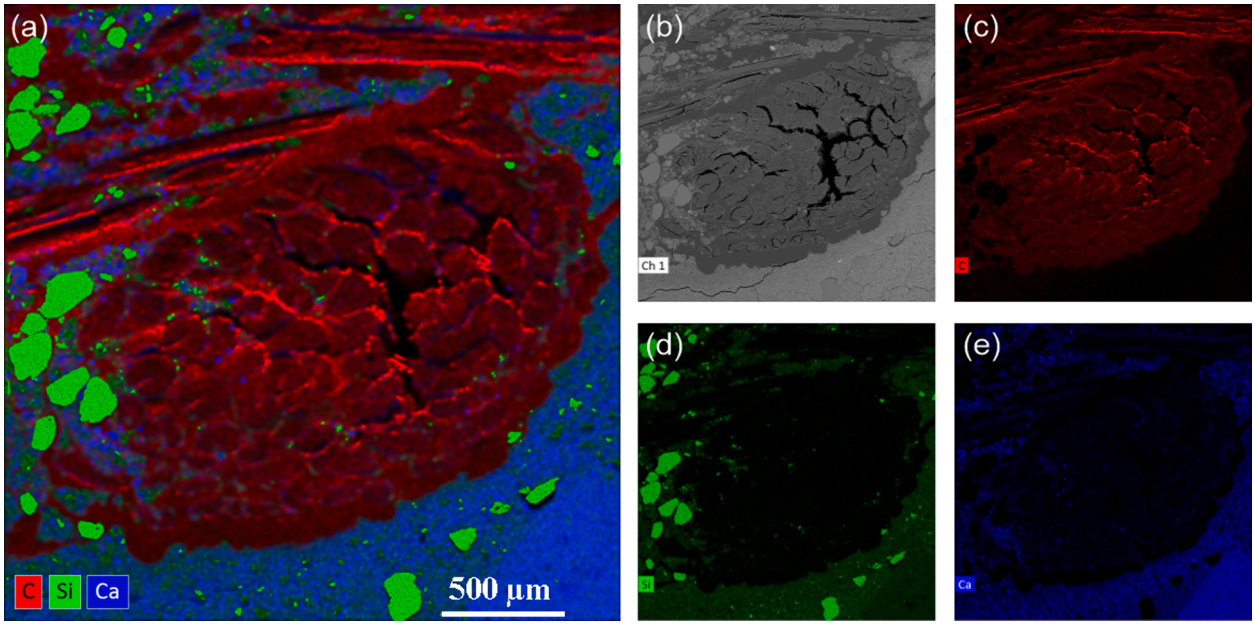

Fig. 11. EDS elemental mapping of the yarn-matrix interaction for the TRC_REF. The elements C, Si and Ca are indicated by red, green and blue, respectively. (For interpretation of the references to colour in this figure legend, the reader is referred to the web version of this article.)

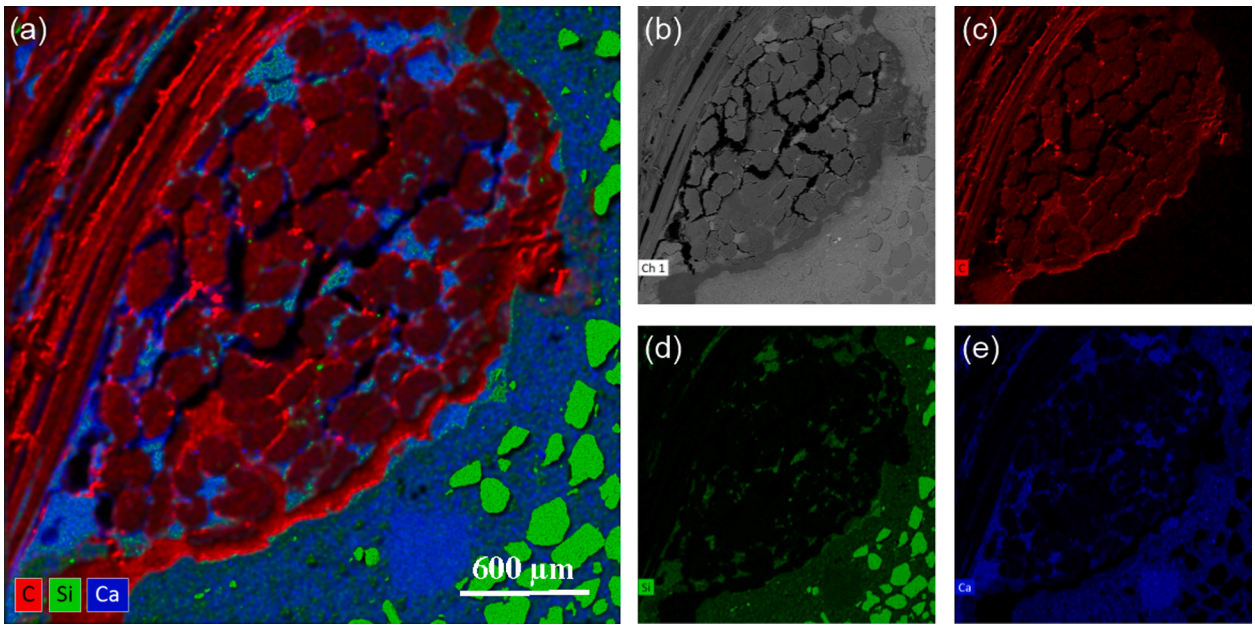

Fig. 12. EDS elemental mapping of the yarn-matrix interaction for the TRC_NS. The elements C, Si and Ca are indicated by red, green and blue, respectively. (For interpretation of the references to colour in this figure legend, the reader is referred to the web version of this article.)

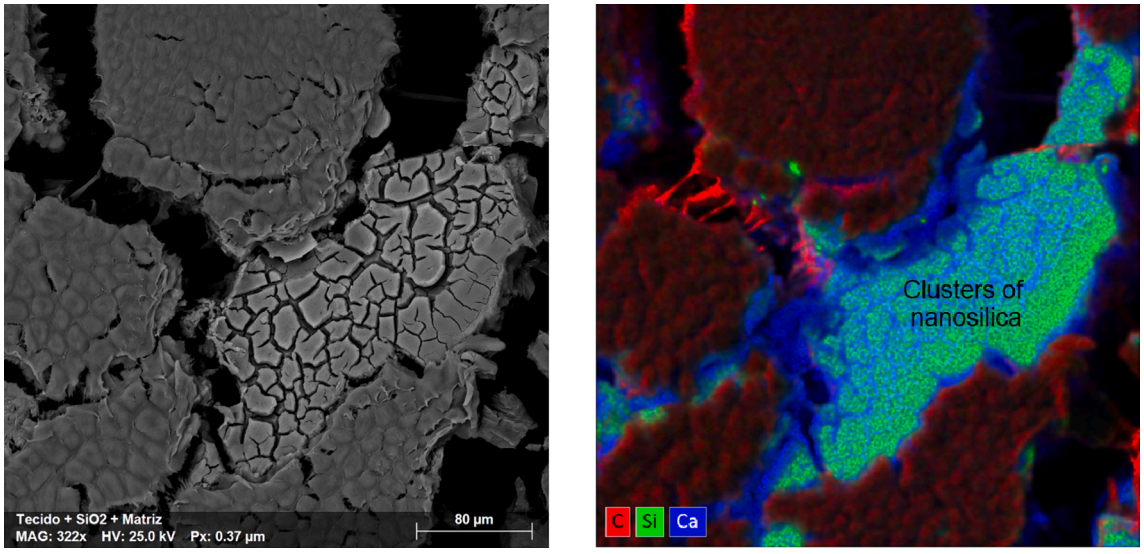

Fig. 13. EDS elemental mapping of the fiber–matrix interaction for the TRC_ NS. The elements C, Si and Ca are indicated by red, green and blue, respectively. (For interpretation of the references to colour in this figure legend, the reader is referred to the web version of this article.)

promote a strain hardening response in the composites tested under tension. Values for the accumulated toughness (up to 4% strain) in these composites were, on average, 1.5 times higher than those obtained for the reference composite and the composite treated with nano-silica. The fibrillation and detachment of fibers from the surface of the fabric changed the 2D nature of the reinforcement to a 3D arrangement enhancing mechanical anchoring with the matrix. In addition, authors believe that these detrimental effects were attributed to the increase of the effective surface area of the yarns and fibers in contact with the matrix. Unfortunately, such assessment was not part of the scope of the study.

The tensile tests showed that the combination of nano-silica and peeling treatments proved to be more effective than the treatments applied independently. In addition to achieving strain hardening behavior, the toughness obtained for the composite using both treatments (up to 4% strain) was more than two times higher in comparison to the reference composite.

Regarding the pull-out test, the treatment with peeling followed by saturation in suspension of nano-silica was found to be the preferable option to be applied to the multifilament sisal yarns when compared to the reference case (saturation with water). These findings are in accordance with the improvements achieved by both treatments applied independently, confirming precisely the trend observed in the direct tensile tests.

It is believed that natural fabrics have a great future in the production and reinforcement of structural and non-structural elements. In this sense, future research on the applicability of this type of composite, taking into account its low modulus and high strain capacity, are extremely necessary.

CRediT authorship contribution statement

Dimas Alan Strauss Rambo: Conceptualization, Methodology, Formal analysis, Resources, Data curation, Writing - original draft, Supervision, Project administration, Funding acquisition. **Caroline Umbinger Oliveira:** Writing - original draft, Methodology, Validation, Data curation, Investigation. **Renan Pícolo Salvador:** Resources, Writing - review & editing, Visualization. **Romildo Dias Toledo Filho:** Methodology, Writing - review & editing. **Otávio Fonseca Martins Gomes:** Investigation, Data curation, Writing - original draft. **Flávio Andrade Silva:** Methodology, Investigation, Data curation, Writing - review & editing. **Mylene Melo Vieira:** Writing - review & editing.

Declaration of Competing Interest

The authors declare that they have no known competing financial interests or personal relationships that could have appeared to influence the work reported in this paper.

Acknowledgements

This work was supported by the Brazilian National Council for Scientific and Technological Development (CNPq) (Universal Call MCTIC/CNPq N° 28/2018 – grant nunber 421509/2018-0). We thank our student Mayara Nayla dos Santos Lopes (São Judas Tadeu University, São Paulo, Brazil) for her contribution to the pull-out measurements. Finally, the authors also thank the Ânima Institute – AI for their support and infrastructure.

References:

[1] A. Peled. Textile Fibre Composites in Civil Engineering, Chapter 4: Bonds in textile-reinforced concrete composites. (2016). Doi: 10.1016/B978-1-78242-446-8.00005-7.
[2] L.O.d. Souza, L.M.S.d. Souza, F. de Andrade Silva, Mechanical autogenous recovery and crack sealing of natural curauá textile reinforced concrete, Constr. Build. Mater. 235 (2020) 117476, https://doi.org/10.1016/j.conbuildmat.2019.117476.
[3] L.O. Souza, L.M.S. Souza, F.A. Silva, Mechanics and cracking mechanisms in natural curauá textile reinforced concrete, RILEM Bookseries. (2018). Doi: 10.1007/978-94-024-1194-2_42.
[4] G. Ferrara, M. Pepe, E. Martinelli, R.D. Tolêdo Filho, Tensile behavior of flax textile reinforced lime-mortar: Influence of reinforcement amount and textile impregnation, Cem. Concr. Compos. 119 (2021) 103984. Doi: 10.1016/j.cemconcomp.2021.103984.
[5] G. Ferrara, C. Caggegi, E. Martinelli, A. Gabor, Shear capacity of masonry walls externally strengthened using Flax-TRM composite systems: experimental tests and comparative assessment, Constr. Build. Mater. 261 (2020) 120490. Doi: 10.1016/j.conbuildmat.2020.120490.
[6] G. Ferrara, C. Caggegi, A. Gabor, E. Martinelli, Flax Textile Reinforced Mortars: Experimental Characterization and Structural Behavior, in: 2020: pp. 885–892. Doi: 10.1007/978-3-030-30938-1_69.
[7] C.B. de Carvalho Bello, I. Boem, A. Cecchi, N. Gattesco, D.V. Oliveira, Experimental tests for the characterization of sisal fiber reinforced cementitious matrix for strengthening masonry structures, Constr. Build. Mater. 219 (2019) 44–55, https://doi.org/10.1016/j.conbuildmat.2019.05.168.
[8] P. Sadrolodabaee J. Claramunt M. Ardanuy A. de la Fuente Characterization of a textile waste nonwoven fabric reinforced cement composite for non-structural building components Constr. Build. Mater. 276 2021 122179 https://doi.org/https://doi.org/10.1016/j.conbuildmat.2020.122179.
[9] Y. Li, Y.-W. Mai, L. Ye, Sisal fibre and its composites: A review of recent developments, Compos. Sci. Technol. 60 (11) (2000) 2037–2055, https://doi.org/10.1016/S0266-3538(00)00101-9.
[10] J. Claramunt, M. Ardanuy, Using vegetable fiber nonwovens cement composites as sustainable materials for applications on ventilated façade systems, in: H. Savastano, J. Fiorelli, S.F. dos Santos (Eds.), Sustain. Nonconv. Constr. Mater. Using Inorg. Bond. Fiber Compos. 2017, pp. 385-397. Doi: 10.1016/B978-0-08-102001-2.00016-4.
[11] , R. L. S. ANELLI. As cidades e o aquecimento global: desafios para o planejamento urbano, as engenharias e as ciências sociais e básicas J. Urban Technol. Sustainab. 3 (2020) 4 17 Doi: 10.47842/juts.v3i1.17.
[12] D.B. Dittenber, H.V.S. GangaRao, Critical review of recent publications on use of natural composites in infrastructure, Compos. Part A Appl. Sci. Manuf. 43 (8) (2012) 1419–1429, https://doi.org/10.1016/j.compositesa:2011.11.019.
[13] G.H.D. Tonoli, A.P. Joaquim, M.-A. Arsène, K. Bilba, H. Savastano, Performance and durability of cement based composites reinforced with refined sisal pulp, Mater. Manuf. Process. 22 (2) (2007) 149–156, https://doi.org/10.1080/10426910601062065.
[14] S.R. Ferreira, F.D.A. Silva, P.R.L. Lima, R.D. Toledo Filho, Effect of fiber treatments on the sisal fiber properties and fiber-matrix bond in cement based systems, Constr. Build. Mater. 101 (2015) 730–740, https://doi.org/10.1016/j.conbuildmat.2015.10.120.
[15] M.F.M. Freitas, Desenvolvimento de processo de alinhamento magnético de fibras curtas de sisal em matriz cimentícia e influência no comportamento mecânico, Master's thesis, São Judas Tadeu University, São Paulo, 2020.
[16] F.A. Silva, N. Chawla, R.D. de, T. Filho, Tensile behavior of high performance natural (sisal) fibers, Compos. Sci. Technol. 68 (2008) 3438–3443, https://doi.org/10.1016/j.compscitech.2008.10.001.
[17] R.S. Olivito, O.A. Cevallos, A. Carrozzini, Development of durable cementitious composites using sisal and flax fabrics for reinforcement of masonry structures, Mater. Des. 57 (2014) 258–268, https://doi.org/10.1016/j.matdes.2013.11.023.
[18] Flávio.de.A. Silva, M. Butler, V. Mechtcherine, D. Zhu, B. Mobasher, Strain rate effect on the tensile behaviour of textile-reinforced concrete under static and dynamic loading, Mater. Sci. Eng. A. 528 (3) (2011) 1727–1734, https://doi.org/10.1016/j.msea.2010.11.014.
[19] A. Peled, A. Bentur, D. Yankelevsky, Effects of woven fabric geometry on the bonding performance of cementitious composites: mechanical performance, Adv. Cem. Based Mater. 7 (1) (1998) 20–27, https://doi.org/10.1016/S1065-7355(97)00012-6.
[20] R. Alagirusamy, A. Das, Yarns: Production, processability and properties. Fibrous and Composite Materials for Civil Engineering Applications, in: R. Fangueiro (Eds.) Fibrous and composite materials for civil engineering applications, Woodhead Publishing, 2011, pp. 29–61. doi:10.1533/9780857095583.1.29.
[21] J.A. Melo Filho, F.A. Silva, R.D. Toledo Filho, E.M.R., Fairbairn, Effect of Reinforcement Ratio and Molding Pressure on the Mechanical Performance of Short Sisal FRC, In: 4th International Conference on Science and Technology of Composite Materials, 2007. Rio de Janeiro – RJ (2007).
[22] G.C. Yang, H.M. Zeng, J.J. Li, N.B. Jian, W.B. Zhang, Relation of modification and tensile properties of sisal fibre, Acta Scientiarum Naturalium Universitatis Sunyatseni 35 (1996) 53.
[23] S.R. Ferreira, Flávio.de.A. Silva, P.R.L. Lima, R.D. Toledo Filho, Effect of hornification on the structure, tensile behavior and fiber matrix bond of sisal, jute and curauá fiber cement based composite systems, Constr. Build. Mater. 139 (2017) 551–561, https://doi.org/10.1016/j.conbuildmat.2016.10.004.
[24] A. Neves Junior, S.R. Ferreira, R.D. Toledo Filho, E.de.M.R. Fairbairn, J. Dweck, Effect of early age curing carbonation on the mechanical properties and durability of high initial strength Portland cement and lime-pozolan composites reinforced with long sisal fibres, Compos. Part B Eng. 163 (2019) 351–362, https://doi.org/10.1016/j.compositesb:2018.11.006.
[25] AENOR. UNE-EN 197-1:2011. Cement - Part 1: Composition, specifications and conformity criteria for common cements, 2011.
[26] ABNT. NBR 7215. Portland cement - Determination of compressive strength of cylindrical test specimens, 2019.
[27] F.A. Silva, B. Mobasher, R.D. Toledo Filho, Fatigue behavior of sisal fiber reinforced cement composites, Mater. Sci. Eng. A. 527 (2010) 5507–5513, https://doi.org/10.1016/j.msea.2010.05.007.
[28] M.H. Maciel, G.Simões. Soares, R.C.de.O. Romano, M.A. Cincotto, Monitoring of Portland cement chemical reaction and quantification of the hydrated products by XRD and TG in function of the stoppage hydration technique, J. Therm. Anal. Calorim. 136 (3) (2019) 1269–1284, https://doi.org/10.1007/s10973-018-7734-5.
[29] R.P. Salvador, D.A.S. Rambo, R.M. Bueno, K.T. Silva, A.D. de Figueiredo, On the use of blast-furnace slag in sprayed concrete applications, Constr. Build. Mater. 218 (2019) 543–555, https://doi.org/10.1016/j.conbuildmat.2019.05.132.
[30] R.T.C. 232-T. (Wolfgang Brameshuber), Recommendation of RILEM TC 232-TDT: test methods and design of textile reinforced concrete, Mater. Struct. 49 (2016) 4923–4927. https://doi.org/10.1617/s11527-016-0839-z.
[31] L. Bjerregaard, K. Geels, B. Ottesen, M. Rückert, Metalog Guide, fourth ed, Denmark, 2002.
[32] J.I. Goldstein, D.E. Newbury, P. Echlin, D.C. Joy, C.E. Lyman, C. Fiori, E. Lifshin, L. Sawyer, J.R. Michael. Scanning Scanning Electron Microscopy and X-ray Microanalysis, third ed., Springer, New York, 2003.
[33] S.F. Santos, R.S. Teixeira, H. Savastano Junior, Interfacial transition zone between lignocellulosic fiber and matrix in cement-based composites, in: H. Savastano, J. Fiorelli, S.F. dos Santos (Eds.), Sustain. Nonconv. Constr. Mater. Using Inorg. Bond. Fiber Compos. 2017, pp. 385-397. https://doi.org/10.1016/B978-0-08-102001-2.00016-4.
[34] M.E.A. Fidelis, Development and mechanical characterization of textile reinforced concrete reinforced with jute fabric, Phd thesis, Federal University of Rio de Janeiro, Rio de Janeiro, 2014.
[35] D.A.S. Rambo, Temperature effect on the mechanical behavior of refractory composites reinforced with basalt and carbon textile, Phd thesis, Federal University of Rio de Janeiro, Rio de Janeiro, 2016.
[36] D. Zhu, B. Mobasher, A. Vaidya, S.D. Rajan, Mechanical behaviors of Kevlar 49 fabric subjected to uniaxial, biaxial tension and in-plane large shear deformation, Compos. Sci. and Tech. 74 (2013) 121–130.
[37] A. Bentur, S. Mindess, Fibre reinforced cementitious composites Second ed. CRC Press Modern Concrete Technology, 1990.
[38] R.S.P. Coutts, A review of Australian research into natural fibre cement composites, Cem. Concr. Comp. 27 (2005) 518–526.
[39] T. Gong, A.H. Ahmed, I. Curosu, V. Mechtcherine, Tensile behavior of hybrid fiber reinforced composites made of strain-hardening cement-based composites (SHCC) and carbon textile, Constr. Build. Mater. 262 (2020) 120913, https://doi.org/10.1016/j.conbuildmat.2020.120913.

[40] R.D. Toledo Filho, Flávio.de.A. Silva, E.M.R. Fairbairn, João.de.A.M. Filho, Durability of compression molded sisal fiber reinforced mortar laminates, Constr. Build. Mater. 23 (6) (2009) 2409–2420, https://doi.org/10.1016/j.conbuildmat.2008.10.012.

[41] J.A. Melo Filho, F.A. Silva, R.D. Toledo Filho, Degradation kinetics and aging mechanisms on sisal fiber cement composite systems, Cem. Concr. Comp. 40 (2014) 30–39, https://doi.org/10.1016/j.cemconcomp.2013.04.003.

[42] A. Peled, V. Mechtcherine, D. Nicke, S. Hempel. Modifying carbon roving cement matrix bond by inorganic coating. In: Seventh International RILEM Conference on High Performance Fiber Reinforced Cement Composites (HPFRCC7), Stuttgart, 2015, pp. 61-68.